Supporting information for:

Title: Activationless Multiple-Site Concerted Proton-Electron Tunneling

Authors: Miriam A. Bowring[1,2,3]*, Liam R. Bradshaw[2], Giovanny A. Parada[1], Timothy P. Pollock[2], Ricardo J. Fernández-Terán[4], Scott S. Kolmar[1], Brandon Q. Mercado,[1] Cody W. Schlenker[2], Daniel R. Gamelin[2], James M. Mayer[1,2]*

Affiliations:
[1] Department of Chemistry, Yale University, New Haven, CT 06520, USA
[2] Department of Chemistry, University of Washington, Seattle, WA 98195, USA
[3] Department of Chemistry, Reed College, Portland, OR 97202, USA
[4] Department of Chemistry, Ångström Laboratory, Uppsala University, Box 523, SE 75120 Uppsala, Sweden

* Correspondence to: mbowring@reed.edu, james.mayer@yale.edu

Table of Contents:

1. Synthesis.

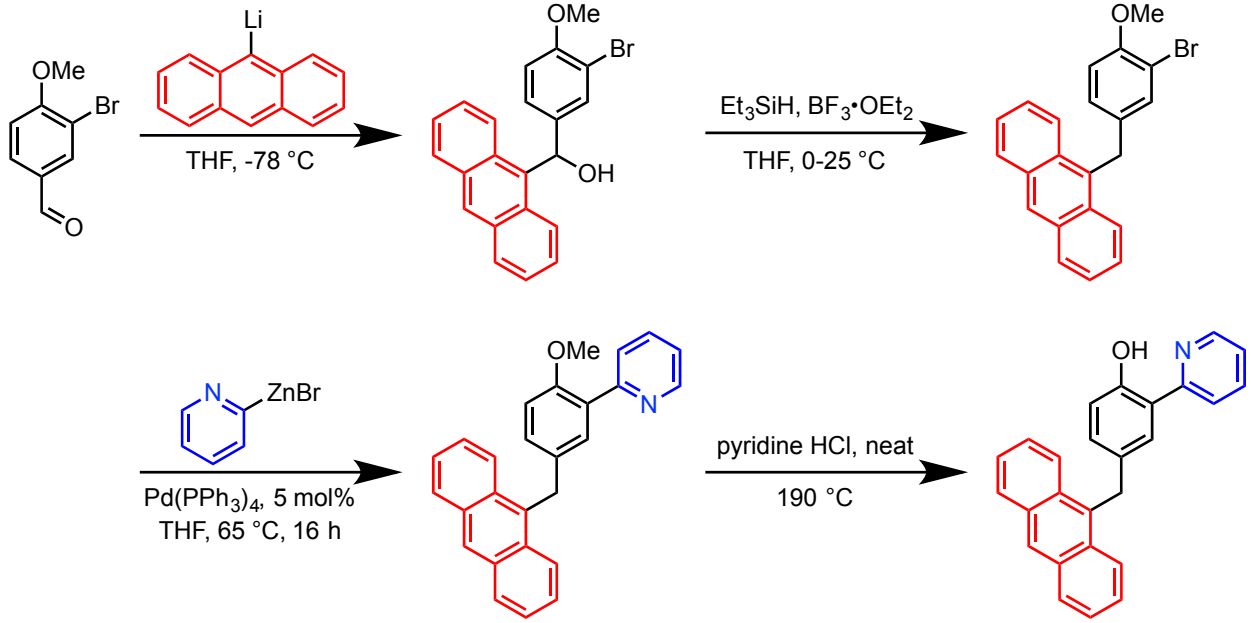

Scheme S1. Synthetic route to **1H**.

General Synthetic Considerations.
All reactions were conducted under a nitrogen or argon atmosphere using standard Schlenk techniques or a nitrogen or argon atmosphere glovebox. Purification procedures were conducted in air. Reaction solvents were dried using a Glass Contour solvent purification system or by distillation under nitrogen from appropriate drying agents. 2-bromo-4-methoxybenzaldehyde (Aldrich), 9-bromoanthracene (Aldrich), *n*-butyllithium (Aldrich), Et_3SiH (Aldrich), $BF_3{\cdot}OEt_2$ (Aldrich), 2-pyridyl zinc bromide (Aldrich), $Pd(PPh_3)_4$ (Strem), and pyridine·HCl (Aldrich) were purchased and used without further purification. NMR spectra were recorded on Bruker spectrometers at room temperature. Spectra were referenced internally by the residual solvent proton signal for ^1H NMR and by the solvent signal for ^{13}C NMR spectra. UV-vis spectra were collected on a Hewlett Packard 8453 diode array spectrophotometer. Elemental analyses were performed by Robertson Microlit Laboratories, Ledgewood, NJ. Samples for high resolution mass spectrometry were prepared in acetonitrile with 0.05% formic acid. Solutions were directly injected (at 6 µL/min flow using a 500µL Hamilton Syringe) into an Orbitrap XL mass spectrometer (ThermoFisher Scientific) via API electrospray source. The ionization source parameters were: ESI voltage (4 kV); tube lens (125 V); capillary temperature (300 °C) and voltage (20 V); auxiliary and sheath gas flow rate (10 and 11, respectively). MS data were collected in profile mode at a resolution of 100,000 in the Orbitrap detector and for 10 scans in positive mode conditions. The resulting mass spectra are averages over 10 scans. Peak picking and analyses were carried out with Xcalibur Software (v. 2.6).

4-(9-anthrylmethyl)-2-(2-pyridinyl)anisole (**1Me**)

9-Bromoanthracene (3.0 g, 12 mmol) was dissolved in dry THF (24 mL), and the solution was stirred and cooled to -78 °C. A solution of *n*-butyllithium (2.5 M, 4.9 mL, 13 mmol) in hexane was added dropwise. After 30 min, 2-bromo-4-methoxybenzaldehyde (2.5 g, 12 mmol) was added dropwise as a solution in THF (12 mL). After 15 min, the flask was allowed to warm to

22 °C, and then saturated aqueous NH_4Cl (20 mL) was added. The organic layer was separated, and the aqueous layer was extracted with EtOAc twice. The combined organic layers were washed with brine and dried over $MgSO_4$. The residue was purified by silica gel column chromatography (7:1 hexanes:EtOAc followed by 4:1 hexanes:THF). The product was precipitated from EtOAc with hexanes to yield a yellow powder (1.8 g).

The powder (1.7 g, ~4.3 mmol) was dissolved in CH_2Cl_2 (150 mL), and the resulting solution was cooled to -60 °C. Et_3SiH (1.7 mL, 11 mmol) and $BF_3{\cdot}OEt_2$ (0.9 mL, 7 mmol) were added. The solution was stirred for 1 h, then allowed to warm to 22 °C. Saturated aqueous Na_2CO_3 was added. The organic layer was separated, and the aqueous layer was extracted with CH_2Cl_2 twice. The combined organic layers were washed with brine and dried over $MgSO_4$, yielding a yellow solid (1.2 g).

The yellow solid (1.0 g, ~2.7 mmol) and $Pd(PPh_3)_4$ (0.15 g, 0.13 mmol) were dissolved in THF (12 mL). 2-Pyridyl zinc bromide (13.3 mL, 0.5 M, 7 mmol) in THF was added. The mixture was stirred at 65 °C for 18 h, then allowed to cool to 22 °C. Water (30 mL) was added, and the resulting mixture was extracted with EtOAc (20 mL) three times and CH_2Cl_2 (30 mL) three times. The organic layers were dried over $MgSO_4$. One portion of the residue (crude **1Me**, 330 mg) was purified by silica gel column chromatography (3:1 hexanes:EtOAc with 0.1% NEt_3) to yield the white solid **1Me (**88 mg, 3% yield over 3 steps).

Anal. Calcd. for $C_{27}H_{21}NO$: C, 86.37; H, 5.64; N, 3.73. Found: C, 85.35; H, 5.59; N, 3.51.

^{1}H NMR (300 MHz, $CDCl_3$) δ 8.75 (d, J = 5.0 Hz, 1H), 8.44 (s, 1H), 8.30-8.00 (m, 4H), 7.86 (s, 1H), 7.84-7.70 (m, 2H), 7.51-7.41 (m, 4H), 6.80-6.68 (m, 2H), 5.03 (s, 2H), 3.75 (s, 3H). One aromatic resonance was apparently obscured due to coincidental overlap with residual solvent signal.

^{13}C NMR (126 MHz, $CDCl_3$) δ 156.30, 155.44, 149.58, 135.75, 133.42, 132.18, 131.84, 131.01, 130.73, 129.26, 129.22, 126.62, 126.02, 125.36, 125.09, 125.07, 121.82, 111.70, 55.80, 32.84.

UV-Vis (MeCN) λ (nm): 333, 349, 368, 388.

4-(9-anthrylmethyl)-2-(2-pyridinyl)phenol (**1H**)

A portion of the residue of crude **1Me** (75 mg, ~0.2 mmol) was combined with pyridine·HCl (245 mg, 2.1 mmol), and this mixture was melted and stirred at 190 °C for 16 h. Water (0.1 mL) was added, followed by $CDCl_3$ (3 mL). The organic layer was separated, and the brown residue was purified by silica gel column chromatography (5:1 hexanes:EtOAc), yielding the white crystalline product **1H** (30 mg, 12% yield over four steps). Slow vapor diffusion of heptanes into a solution of **1H** in $CHCl_3$ afforded needles suitable for X-ray crystallography. The structure of compound **1H** was confirmed by X-ray crystallography.

Anal. Calcd. for $C_{26}H_{19}NO$: C, 86.40; H, 5.30; N, 3.88. Found: C, 85.79; H, 5.40; N, 3.78.

^{1}H NMR (500 MHz, THF-d_8) δ 13.68 (br s, 1H), 8.49-8.46 (m, 2H), 8.33 (d, J = 8 Hz, 2H), 8.04 (d, J = 8 Hz, 2H), 7.80-7.72 (m, 3H), 7.48-7.41 (m, 4H), 7.22 (dd, J = 6 Hz, 1H), 6.95 (d, J = 9 Hz, 1H), 6.71 (d, J = 9 Hz, 1H), 5.02 (s, 2H).

^{13}C NMR (126 MHz, $CDCl_3$) δ 158.4, 158.0, 146.0, 137.7, 132.2, 131.9, 131.6, 131.1, 130.8, 129.3, 126.7, 126.1, 125.6, 125.1, 125.0, 121.4, 119.2, 118.8, 33.1.

UV-Vis (MeCN) λ (nm): 333, 350, 368, 388.

HRMS m/z: 361.15 (100.0%), 362.15 (28.1%), 363.15 (2.7%), 363.15 (1.1%).

The NMR data below for compounds **1H** and **1Me** confirm the identity of these compounds and indicate that their purity is good. Minor contamination from solvents and from aromatic impurities is observed.

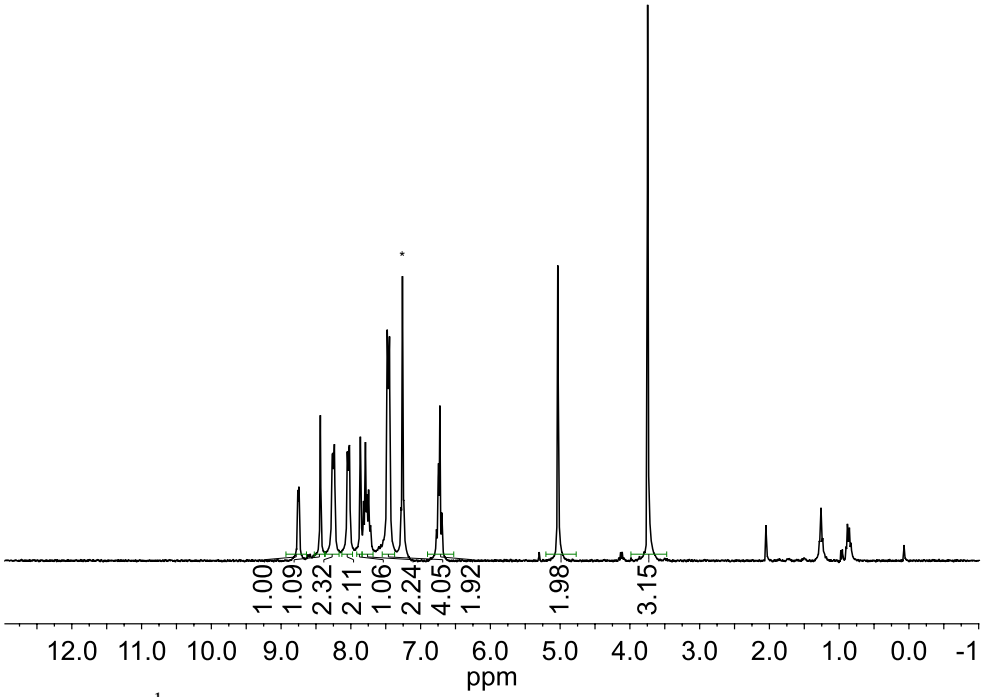

Figure S1. ^{1}H NMR spectrum of **1Me** in $CDCl_3$. Residual solvent signal from $CHCl_3$ is marked with an asterisk.

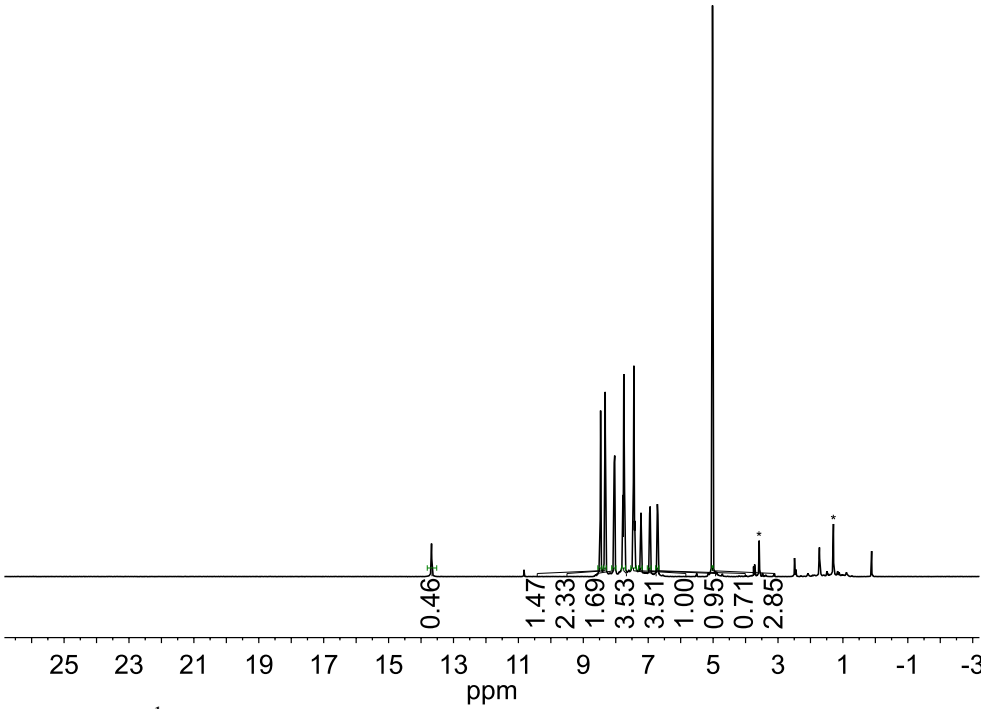

Figure S2. ^{1}H NMR spectrum of **1H** in THF-d_8. Residual solvent signals from THF-d_7 are marked with asterisks.

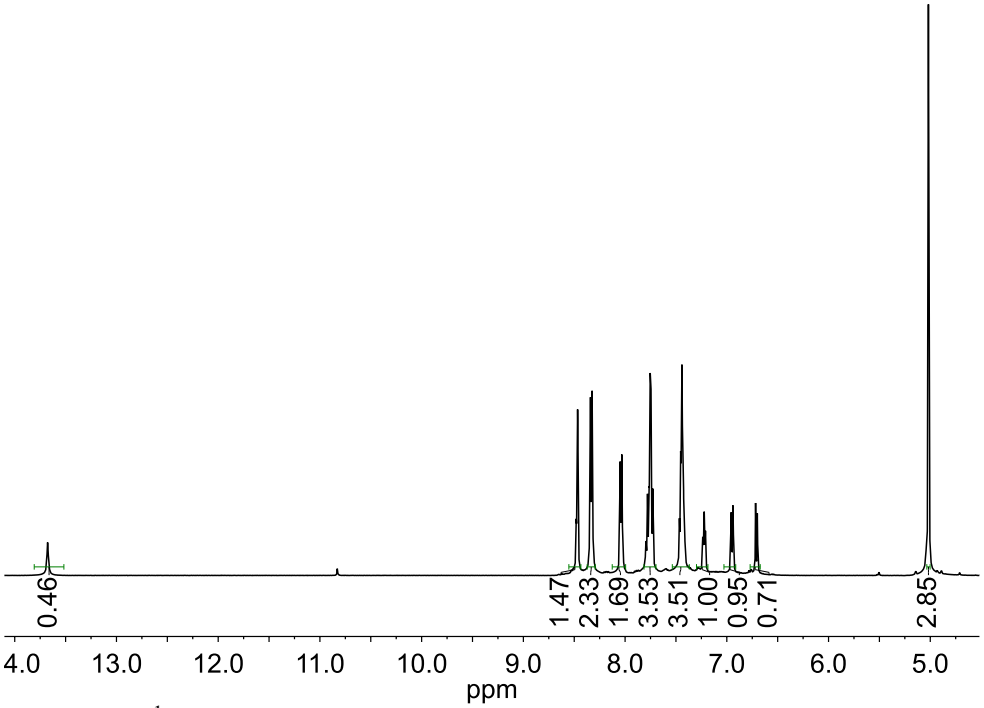

Figure S3. ^{1}H NMR spectrum of **1H** in THF-d_8, enlarged to show detail.

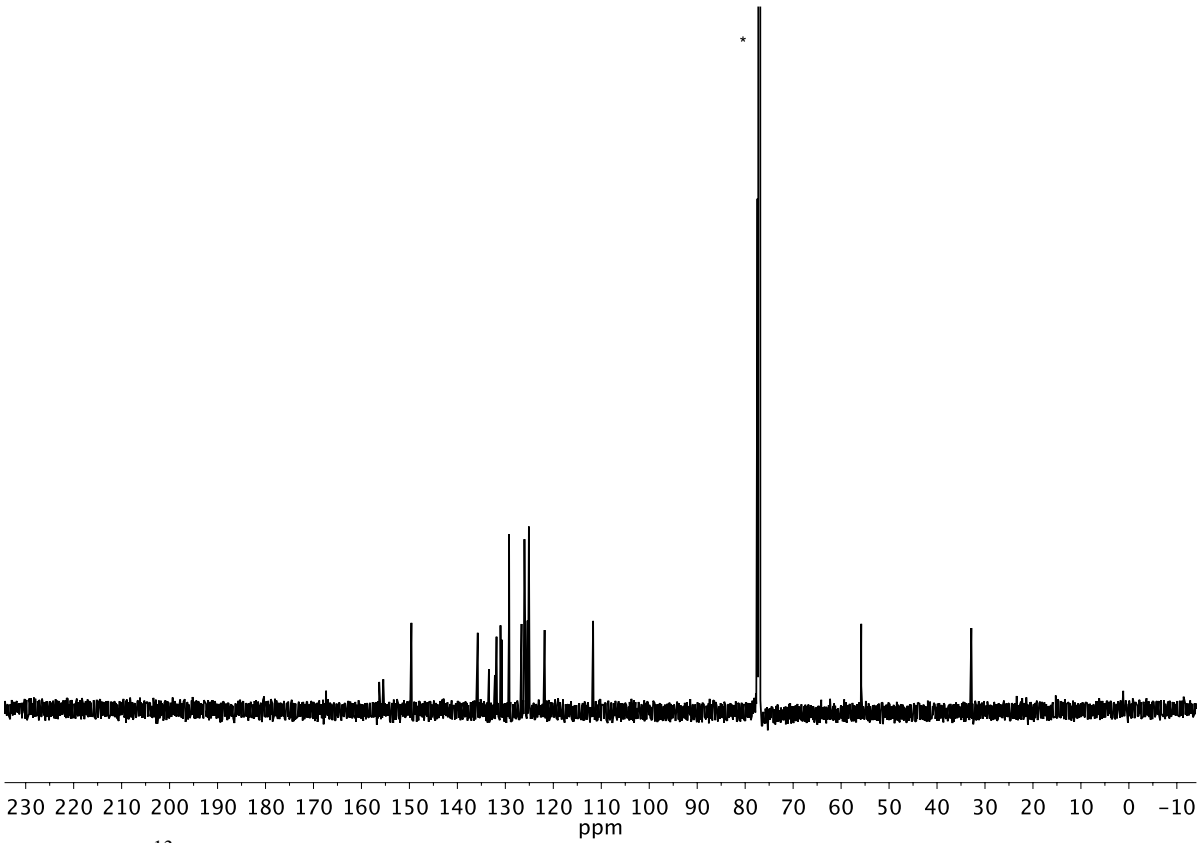

Figure S4. ^{13}C NMR spectrum of **1Me** in $CDCl_3$. Solvent signal is marked with an asterisk.

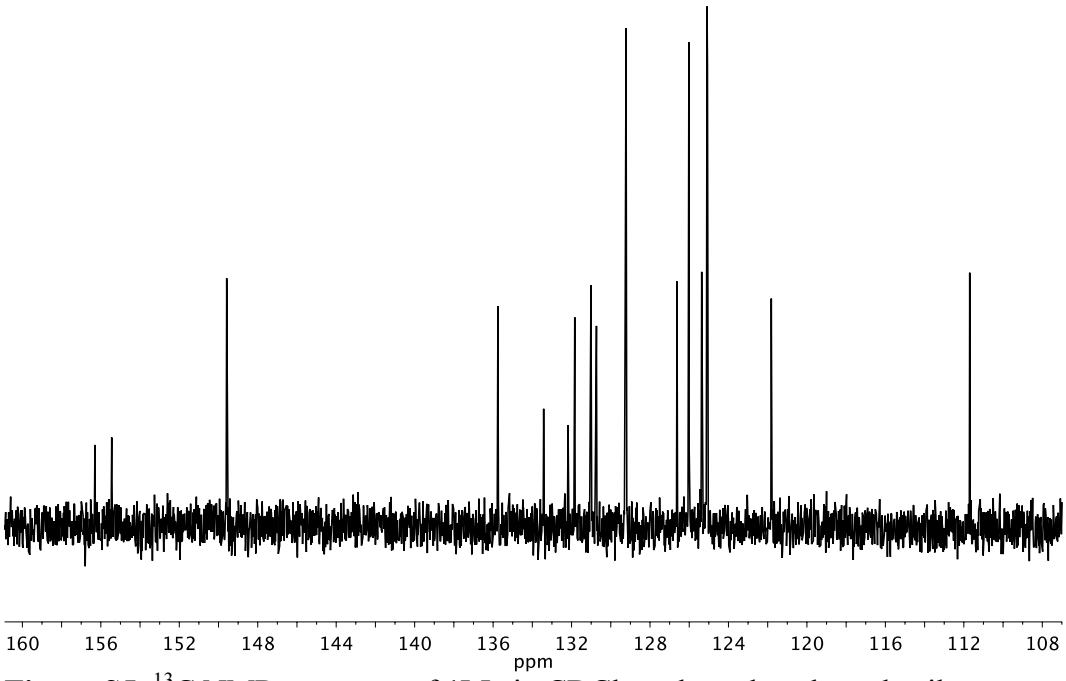

Figure S5. ^{13}C NMR spectrum of **1Me** in $CDCl_3$, enlarged to show detail.

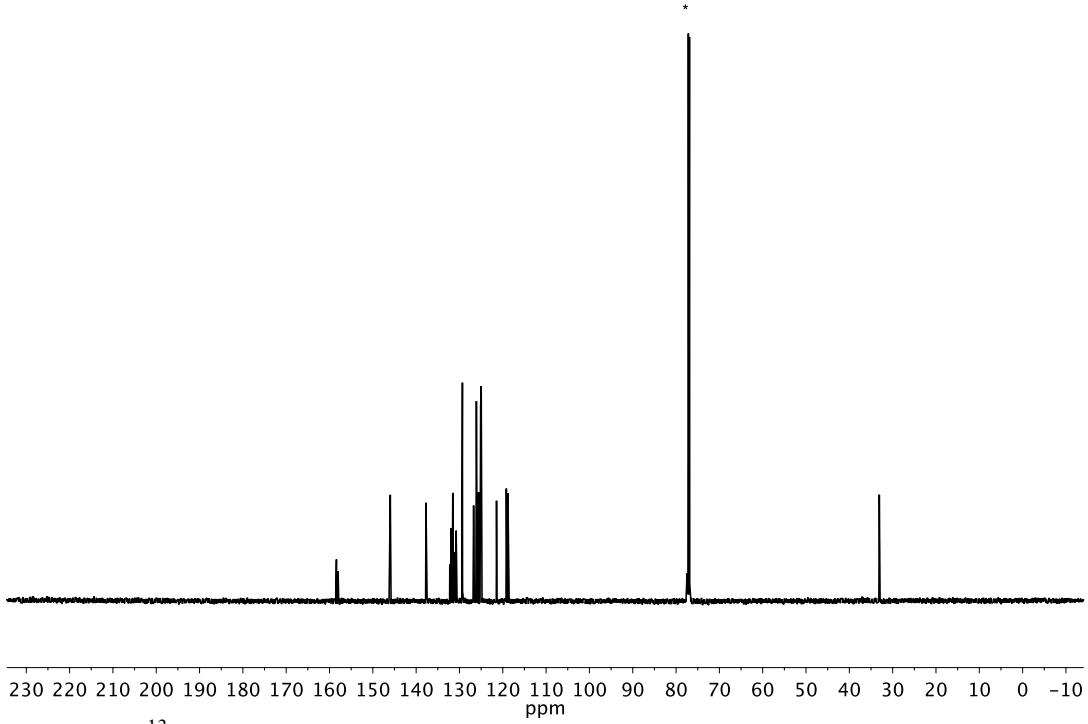

Figure S6. ^{13}C NMR spectrum of **1H** in $CDCl_3$. Solvent signal is marked with an asterisk.

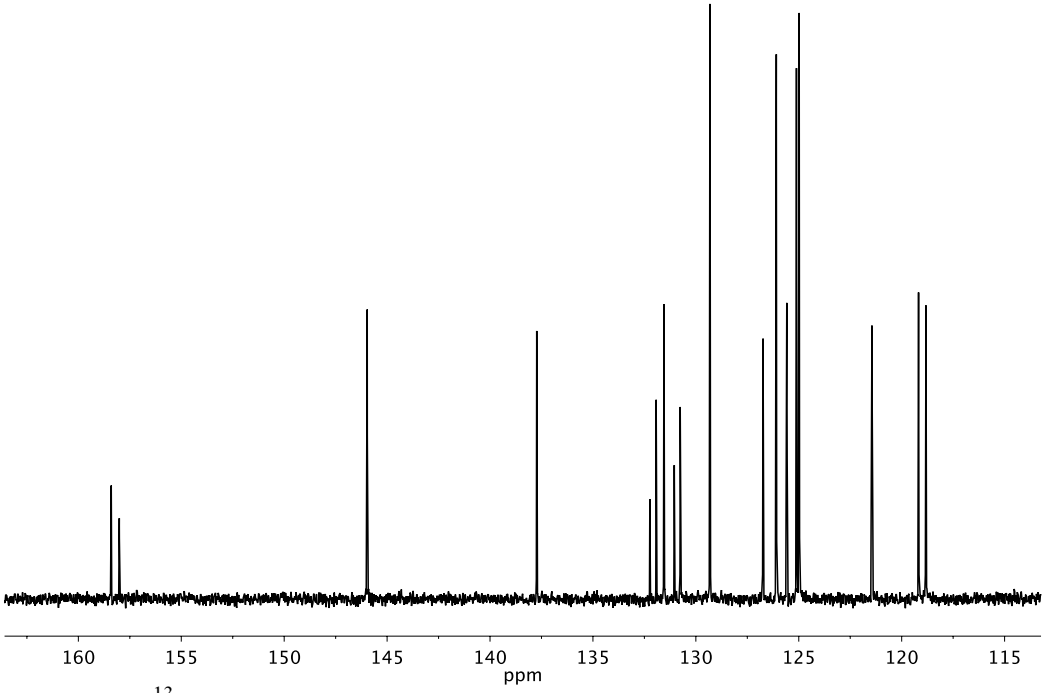

Figure S7. ^{13}C NMR spectrum of **1H** in $CDCl_3$, enlarged to show detail.

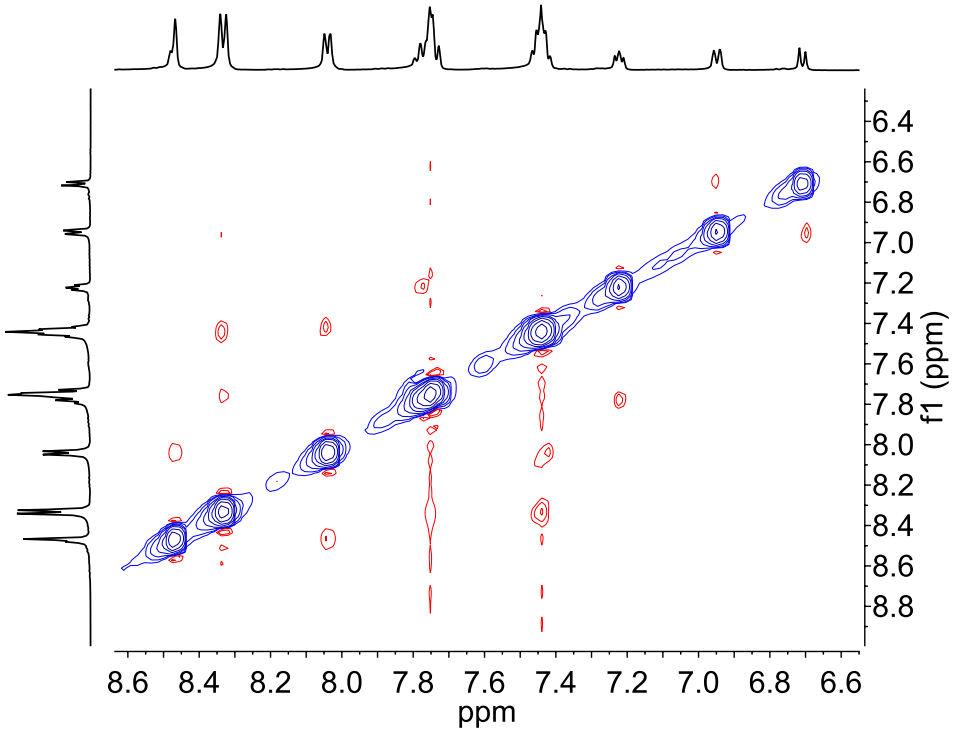

Figure S8. NOESY spectrum of **1H**, aromatic region.

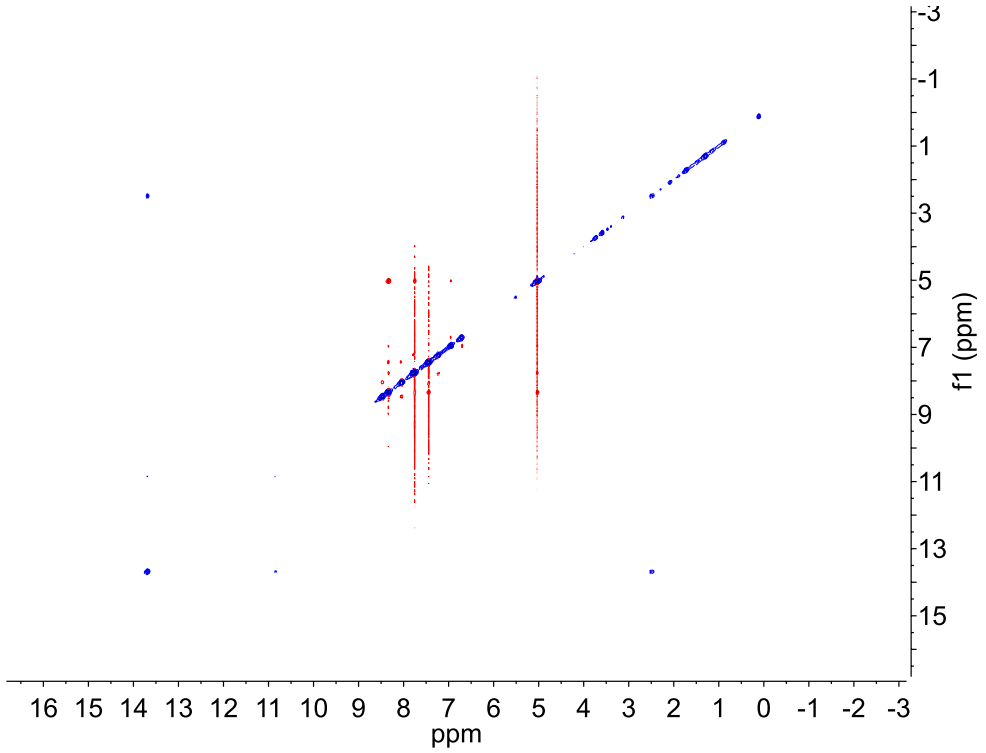

Figure S9. Full NOESY spectrum of **1H**.

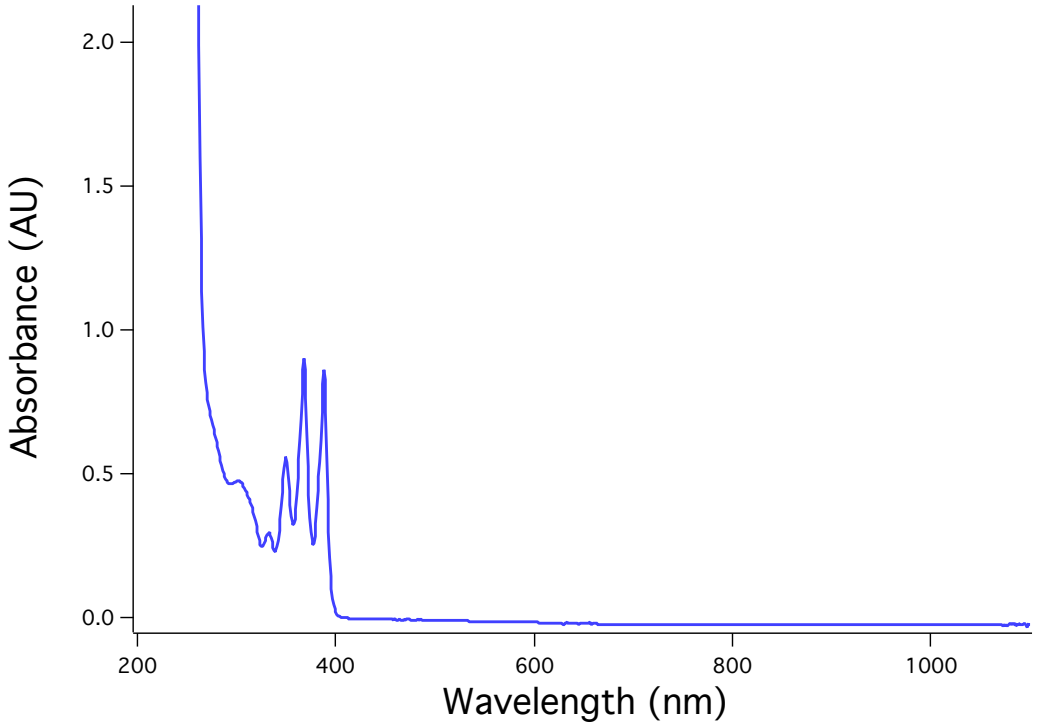

Figure S10. UV-visible absorption spectrum of **1H** (0.10 mM) in MeCN.

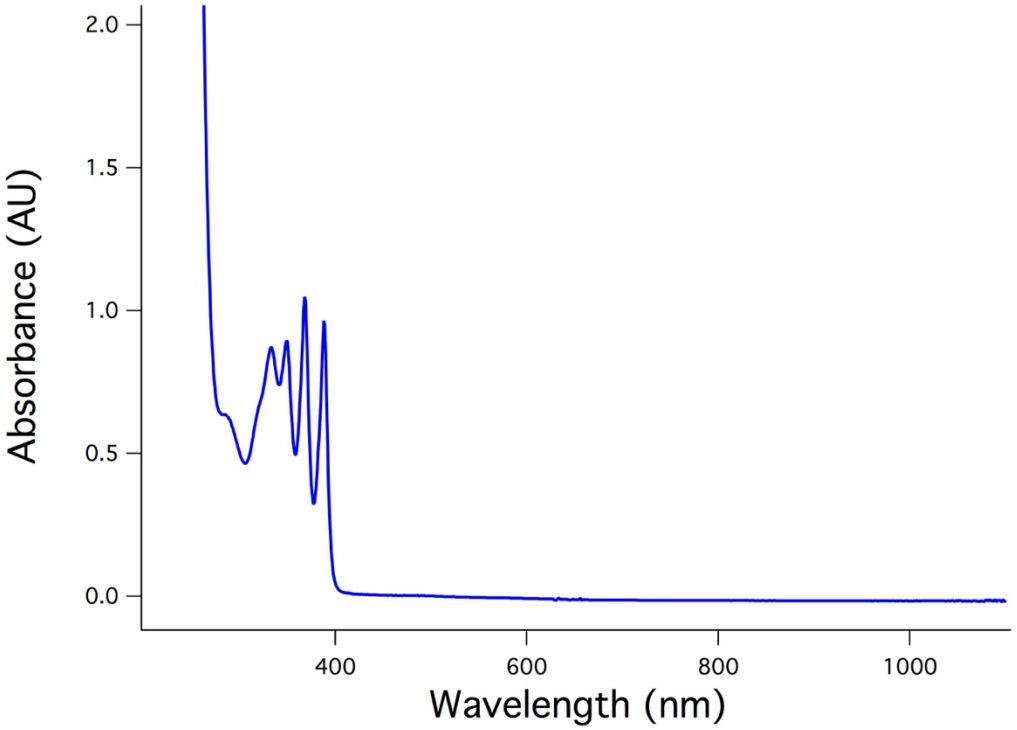

Figure S11. UV-visible absorption spectrum of **1Me** (0.10 mM) in MeCN.

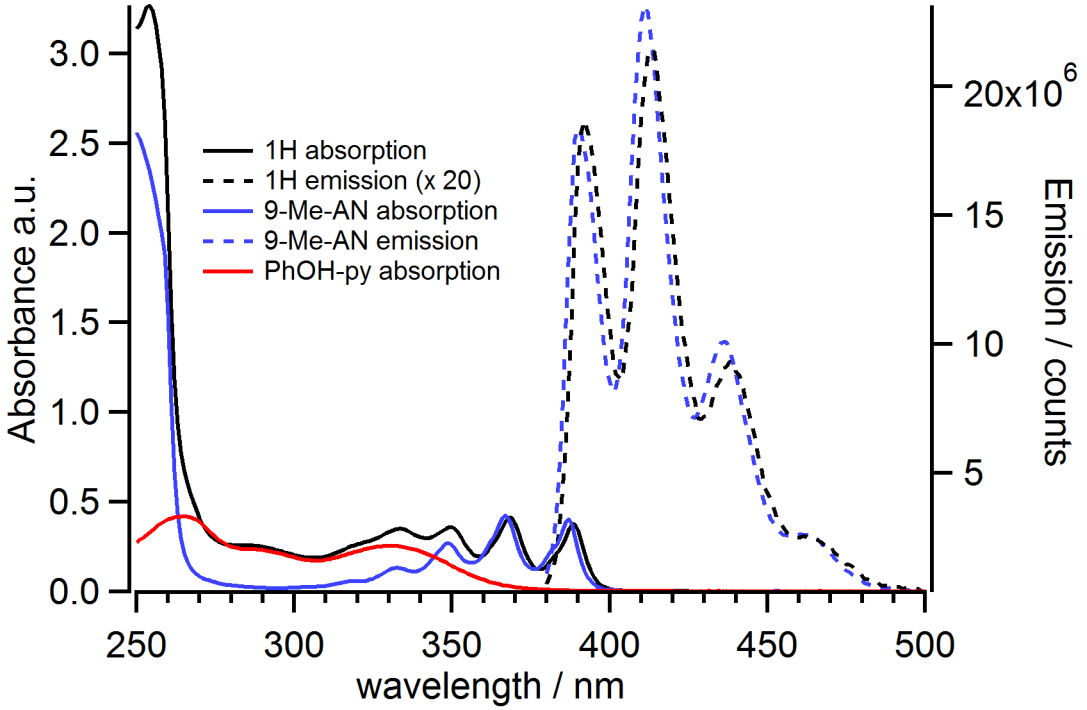

Figure S12. Absorption and emission spectra of **1H**, reference compound 9-methyl-anthracene (9-Me-anth), and reference compound 2,4-di-tertbutyl-6-(pyridin-2-yl)phenol (PhOH-py). Black solid line: UV-vis spectrum of **1H** (0.044 ± 0.010 mM) in MeCN. Black dotted line: steady state emission spectrum of **1H** (0.044 ± 0.010 mM) in MeCN, increased by a factor of 20 to fit the scale. Blue solid line: UV-vis spectrum of 9-Me-anth (0.057 ± 0.010 mM) in MeCN. Blue dotted line: steady state emission spectrum of 9-Me-anth (0.057 ± 0.010 mM) in MeCN. Red solid line: UV-vis spectrum of PhOH-py (0.033 ± 0.011 mM) in MeCN. Steady state emission spectra taken in a Horiba Fluorolog 3 instrument at 365 nm excitation wavelength with slits at 0.1 nm for both excitation and detection monochromators.

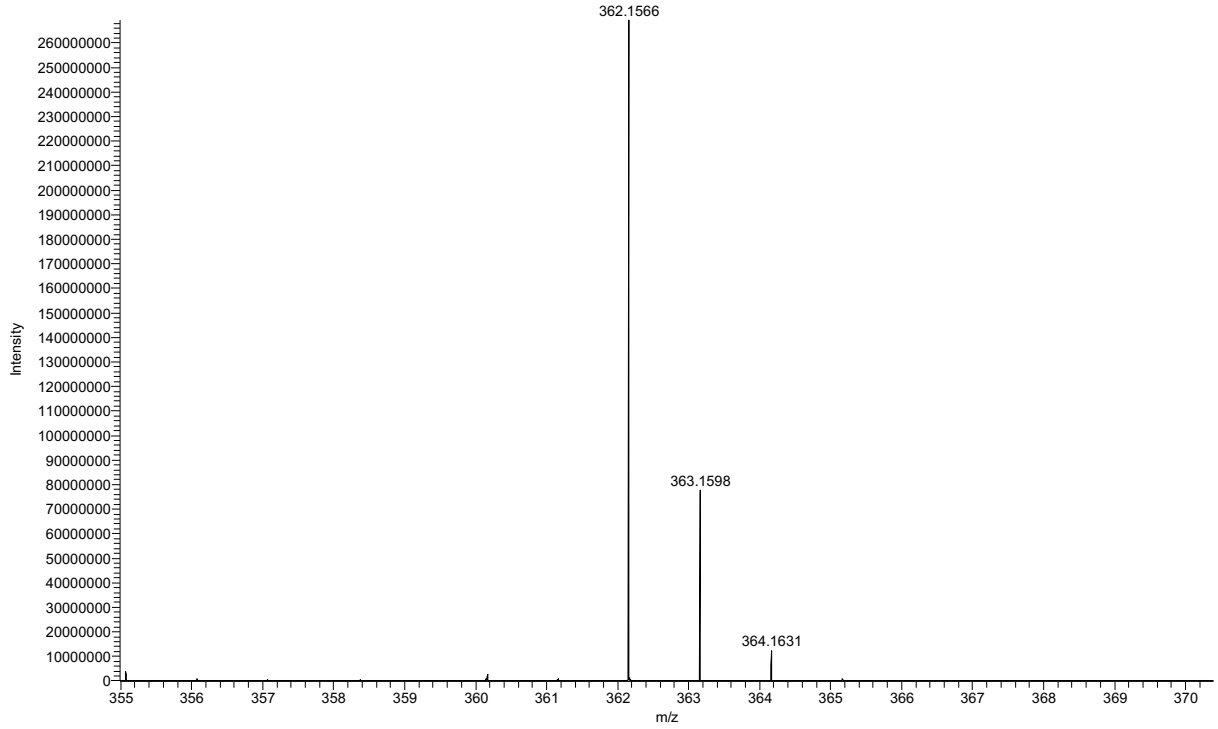

Figure S13. High resolution mass spectrum of **1H**, detail.

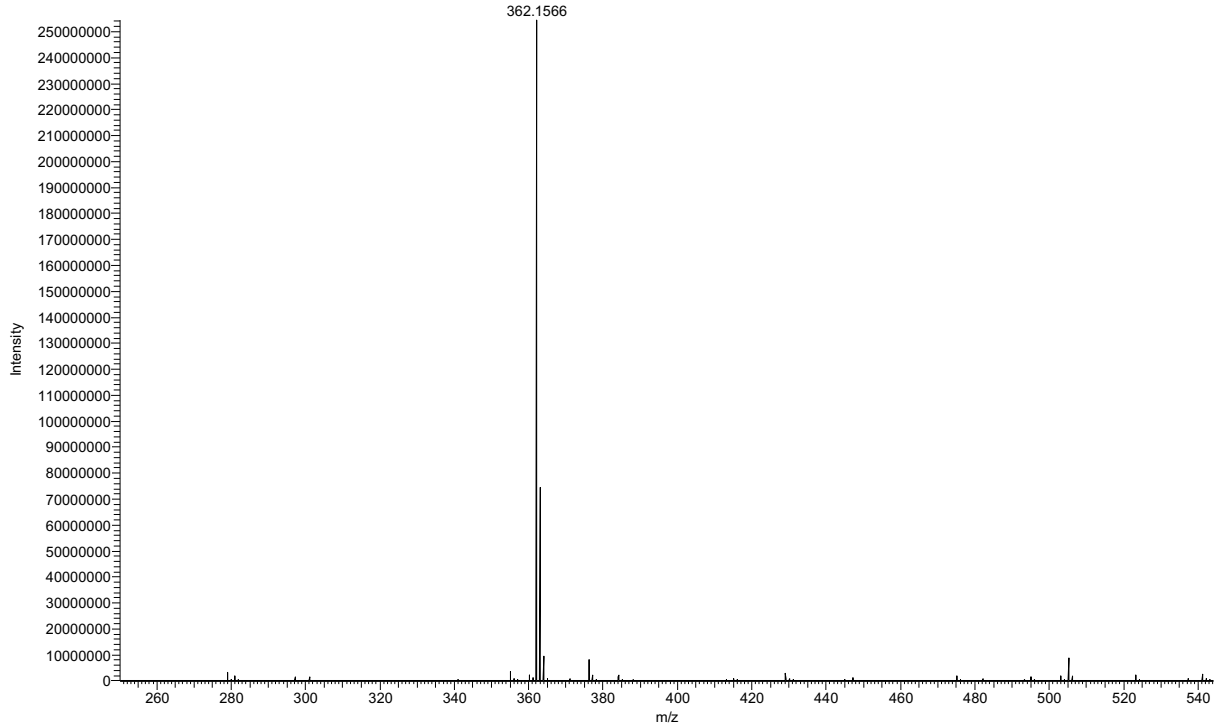

Figure S14. High resolution mass spectrum of **1H**, full spectrum.

2. X-ray crystallographic data.

Experimental and refinement details.

Low-temperature diffraction data (ω-scans) were collected on a Rigaku MicroMax-007HF diffractometer coupled to a Saturn994+ CCD detector with Cu Kα (λ = 1.54178 Å) for the structure of **1H**. The diffraction images were processed and scaled using Rigaku Oxford Diffraction software (CrysAlisPro; Rigaku OD: The Woodlands, TX, 2015). The structure was solved with SHELXT and was refined against F^2 on all data by full-matrix least squares with SHELXL (Sheldrick, G. M. Acta Cryst. 2008, A64, 112–122). All non-hydrogen atoms were refined anisotropically. Hydrogen atoms were included in the model at geometrically calculated positions and refined using a riding model. The isotropic displacement parameters of all hydrogen atoms were fixed to 1.2 times the U value of the atoms to which they are linked (1.5 times for methyl groups). The only exception is H1, which was found in the difference map and semi-freely refined with an O-H distance restraint of 1.00(2) Å. This restraint length is near the value suggested by the difference map. The full numbering scheme of compound **1H** can be found in the full details of the X-ray structure determination (CIF), which is included as Supporting Information. CCDC number 1565052 (**1H**) contains the supplementary crystallographic data for this paper. These data can be obtained free of charge from The Cambridge Crystallographic Data Center via www.ccdc.cam.ac.uk/data_request/cif.

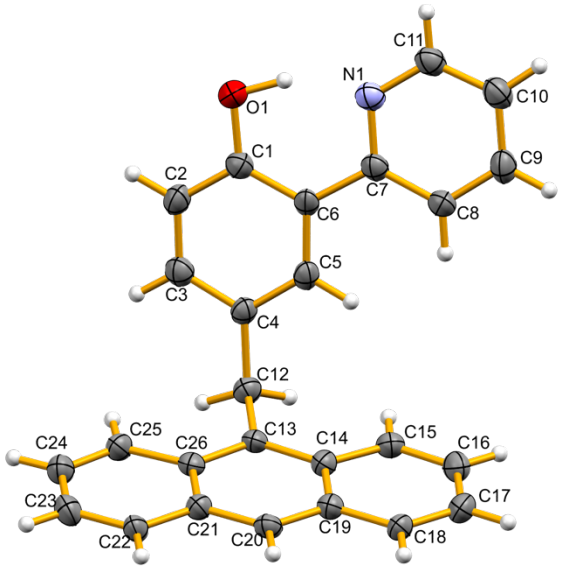

Figure S15. The complete numbering scheme of **1H** with 50% thermal ellipsoid probability levels. The hydrogen atoms are shown as arbitrary circles for clarity.

Table S1. Crystal data and structure refinement for **1H**.

Identification code	007b-17020	
Empirical formula	C26 H19 N O	
Formula weight	361.42	
Temperature	93(2) K	
Wavelength	Cu Kα (1.54184 Å)	
Crystal system	Orthorhombic	
Space group	$Pca2_1$	
Unit cell dimensions	a = 17.7003(8) Å	α = 90°.
	b = 12.0897(6) Å	β = 90°.
	c = 8.2601(4) Å	γ = 90°.
Volume	1767.59(15) Å^3	
Z	4	
Density (calculated)	1.358 Mg/m^3	
Absorption coefficient	0.640 mm^{-1}	
F(000)	760	
Crystal size	0.040 x 0.040 x 0.010 mm^3	
Theta range for data collection	3.656 to 67.380°.	
Index ranges	$-20 \le h \le 21$, $-14 \le k \le 14$, $-9 \le l \le 9$	
Reflections collected	59401	
Independent reflections	3153 [R(int) = 0.1761]	
Completeness to theta = 67.380°	99.2 %	
Absorption correction	Semi-empirical from equivalents	
Max. and min. transmission	1.00000 and 0.40060	
Refinement method	Full-matrix least-squares on F^2	
Data / restraints / parameters	3153 / 2 / 257	
Goodness-of-fit on F^2	1.157	
Final R indices [I>2sigma(I)]	R1 = 0.0679, wR^2 = 0.1546	
R indices (all data)	R1 = 0.0772, wR^2 = 0.1598	
Absolute structure parameter	0.1(5)	
Largest diff. peak and hole	0.218 and –0.234 e.Å^{-3}	

Table S2. Atomic coordinates ($\times 10^4$) and equivalent isotropic displacement parameters ($Å^2 \times 10^3$) for **1H**. U(eq) is defined as one third of the trace of the orthogonalized U^{ij} tensor.

	x	y	z	U(eq)
O(1)	5861(2)	3014(3)	6842(5)	38(1)
N(1)	7269(2)	2518(3)	6984(6)	31(1)
C(1)	6063(3)	3834(4)	5770(6)	30(1)
C(2)	5485(3)	4463(4)	5114(7)	34(1)
C(3)	5646(3)	5303(4)	4019(7)	32(1)
C(4)	6388(3)	5546(4)	3587(6)	26(1)
C(5)	6962(3)	4897(4)	4250(6)	27(1)
C(6)	6826(3)	4032(4)	5346(7)	27(1)
C(7)	7459(3)	3356(4)	5984(6)	28(1)
C(8)	8221(3)	3547(4)	5590(6)	31(1)
C(9)	8778(3)	2868(5)	6223(7)	35(1)
C(10)	8571(3)	2001(4)	7242(7)	37(1)
C(11)	7820(3)	1873(4)	7599(7)	34(1)
C(12)	6576(3)	6483(4)	2414(7)	31(1)
C(13)	6923(3)	7473(4)	3281(6)	27(1)
C(14)	7713(3)	7567(4)	3425(7)	28(1)
C(15)	8242(3)	6824(4)	2697(7)	30(1)
C(16)	9006(3)	6940(4)	2896(7)	34(1)
C(17)	9306(3)	7809(4)	3842(7)	34(1)
C(18)	8825(3)	8548(4)	4550(6)	29(1)
C(19)	8029(3)	8463(4)	4364(6)	28(1)
C(20)	7551(3)	9226(4)	5109(7)	28(1)
C(21)	6764(3)	9162(4)	4932(7)	28(1)
C(22)	6283(3)	9954(4)	5680(7)	30(1)
C(23)	5517(3)	9903(4)	5508(7)	37(1)
C(24)	5198(3)	9048(4)	4541(7)	35(1)
C(25)	5633(3)	8266(4)	3819(7)	31(1)
C(26)	6440(3)	8278(4)	3989(6)	27(1)

Table S3. Bond lengths [Å] and angles [°] for **1H**.

O(1)-C(1)	1.376(6)
O(1)-H(1)	1.02(3)
N(1)-C(11)	1.348(6)
N(1)-C(7)	1.349(6)
C(1)-C(2)	1.385(7)
C(1)-C(6)	1.417(7)
C(2)-C(3)	1.389(7)
C(2)-H(2)	0.9500
C(3)-C(4)	1.393(7)
C(3)-H(3)	0.9500
C(4)-C(5)	1.396(7)
C(4)-C(12)	1.527(7)
C(5)-C(6)	1.404(7)
C(5)-H(5)	0.9500
C(6)-C(7)	1.483(7)
C(7)-C(8)	1.408(7)
C(8)-C(9)	1.384(7)
C(8)-H(8)	0.9500
C(9)-C(10)	1.393(8)
C(9)-H(9)	0.9500
C(10)-C(11)	1.371(8)
C(10)-H(10)	0.9500
C(11)-H(11)	0.9500
C(12)-C(13)	1.524(7)
C(12)-H(12A)	0.9900
C(12)-H(12B)	0.9900
C(13)-C(14)	1.409(7)
C(13)-C(26)	1.421(7)
C(14)-C(15)	1.430(7)
C(14)-C(19)	1.444(7)
C(15)-C(16)	1.370(7)
C(15)-H(15)	0.9500
C(16)-C(17)	1.413(8)
C(16)-H(16)	0.9500

C(17)-C(18)	1.365(7)
C(17)-H(17)	0.9500
C(18)-C(19)	1.421(7)
C(18)-H(18)	0.9500
C(19)-C(20)	1.395(7)
C(20)-C(21)	1.402(7)
C(20)-H(20)	0.9500
C(21)-C(22)	1.423(7)
C(21)-C(26)	1.441(7)
C(22)-C(23)	1.364(7)
C(22)-H(22)	0.9500
C(23)-C(24)	1.423(8)
C(23)-H(23)	0.9500
C(24)-C(25)	1.356(7)
C(24)-H(24)	0.9500
C(25)-C(26)	1.437(7)
C(25)-H(25)	0.9500

C(1)-O(1)-H(1)	103(4)
C(11)-N(1)-C(7)	119.0(4)
O(1)-C(1)-C(2)	117.1(5)
O(1)-C(1)-C(6)	121.9(5)
C(2)-C(1)-C(6)	121.0(5)
C(1)-C(2)-C(3)	120.3(5)
C(1)-C(2)-H(2)	119.8
C(3)-C(2)-H(2)	119.8
C(2)-C(3)-C(4)	121.0(5)
C(2)-C(3)-H(3)	119.5
C(4)-C(3)-H(3)	119.5
C(3)-C(4)-C(5)	117.8(5)
C(3)-C(4)-C(12)	121.6(4)
C(5)-C(4)-C(12)	120.5(4)
C(4)-C(5)-C(6)	123.2(5)
C(4)-C(5)-H(5)	118.4
C(6)-C(5)-H(5)	118.4
C(5)-C(6)-C(1)	116.7(4)

C(5)-C(6)-C(7)	120.7(4)
C(1)-C(6)-C(7)	122.6(5)
N(1)-C(7)-C(8)	120.2(5)
N(1)-C(7)-C(6)	116.3(5)
C(8)-C(7)-C(6)	123.5(5)
C(9)-C(8)-C(7)	119.9(5)
C(9)-C(8)-H(8)	120.1
C(7)-C(8)-H(8)	120.1
C(8)-C(9)-C(10)	119.2(5)
C(8)-C(9)-H(9)	120.4
C(10)-C(9)-H(9)	120.4
C(11)-C(10)-C(9)	118.0(5)
C(11)-C(10)-H(10)	121.0
C(9)-C(10)-H(10)	121.0
N(1)-C(11)-C(10)	123.8(5)
N(1)-C(11)-H(11)	118.1
C(10)-C(11)-H(11)	118.1
C(13)-C(12)-C(4)	111.8(4)
C(13)-C(12)-H(12A)	109.3
C(4)-C(12)-H(12A)	109.3
C(13)-C(12)-H(12B)	109.3
C(4)-C(12)-H(12B)	109.3
H(12A)-C(12)-H(12B)	107.9
C(14)-C(13)-C(26)	120.4(5)
C(14)-C(13)-C(12)	120.2(4)
C(26)-C(13)-C(12)	119.3(4)
C(13)-C(14)-C(15)	124.3(5)
C(13)-C(14)-C(19)	119.3(5)
C(15)-C(14)-C(19)	116.4(4)
C(16)-C(15)-C(14)	122.1(5)
C(16)-C(15)-H(15)	119.0
C(14)-C(15)-H(15)	119.0
C(15)-C(16)-C(17)	120.9(5)
C(15)-C(16)-H(16)	119.5
C(17)-C(16)-H(16)	119.5
C(18)-C(17)-C(16)	119.3(5)

C(18)-C(17)-H(17)	120.4
C(16)-C(17)-H(17)	120.4
C(17)-C(18)-C(19)	121.7(5)
C(17)-C(18)-H(18)	119.2
C(19)-C(18)-H(18)	119.2
C(20)-C(19)-C(18)	120.4(5)
C(20)-C(19)-C(14)	119.9(5)
C(18)-C(19)-C(14)	119.7(5)
C(19)-C(20)-C(21)	121.4(5)
C(19)-C(20)-H(20)	119.3
C(21)-C(20)-H(20)	119.3
C(20)-C(21)-C(22)	120.8(5)
C(20)-C(21)-C(26)	119.5(4)
C(22)-C(21)-C(26)	119.7(4)
C(23)-C(22)-C(21)	121.3(5)
C(23)-C(22)-H(22)	119.4
C(21)-C(22)-H(22)	119.4
C(22)-C(23)-C(24)	119.1(5)
C(22)-C(23)-H(23)	120.5
C(24)-C(23)-H(23)	120.5
C(25)-C(24)-C(23)	121.8(5)
C(25)-C(24)-H(24)	119.1
C(23)-C(24)-H(24)	119.1
C(24)-C(25)-C(26)	121.0(5)
C(24)-C(25)-H(25)	119.5
C(26)-C(25)-H(25)	119.5
C(13)-C(26)-C(25)	123.4(5)
C(13)-C(26)-C(21)	119.5(4)
C(25)-C(26)-C(21)	117.1(4)

Table S4. Anisotropic displacement parameters ($Å^2 \times 10^3$) for **1H**. The anisotropic displacement factor exponent takes the form: $-2\pi^2[h^2 a^{*2}U^{11} + ... + 2 h k a^* b^* U^{12}]$

	U^{11}	U^{22}	U^{33}	U^{23}	U^{13}	U^{12}
O(1)	29(2)	32(2)	52(2)	9(2)	4(2)	-2(2)
N(1)	31(2)	25(2)	37(2)	-2(2)	-3(2)	-1(2)
C(1)	30(3)	24(3)	35(3)	-1(2)	3(2)	0(2)
C(2)	23(3)	33(3)	47(3)	-2(3)	1(3)	-3(2)
C(3)	31(3)	27(3)	39(3)	-4(3)	-2(2)	1(2)
C(4)	22(2)	24(2)	33(3)	-4(2)	-1(2)	-3(2)
C(5)	21(3)	24(3)	37(3)	-8(2)	-2(2)	-2(2)
C(6)	21(2)	18(2)	41(3)	-7(2)	-1(2)	-1(2)
C(7)	27(3)	21(2)	36(3)	-4(2)	-3(2)	0(2)
C(8)	29(3)	23(3)	40(3)	0(2)	3(2)	1(2)
C(9)	24(3)	35(3)	45(3)	-7(3)	-4(2)	3(2)
C(10)	35(3)	28(3)	46(4)	-3(3)	-7(3)	4(2)
C(11)	34(3)	25(3)	41(3)	-1(2)	-7(3)	-1(2)
C(12)	27(3)	26(3)	41(3)	1(2)	-2(2)	-3(2)
C(13)	24(2)	19(3)	38(3)	5(2)	0(2)	0(2)
C(14)	23(3)	26(3)	37(3)	5(2)	-1(2)	-1(2)
C(15)	28(3)	24(3)	37(3)	2(2)	2(2)	-2(2)
C(16)	32(3)	31(3)	39(3)	0(2)	8(3)	5(2)
C(17)	24(3)	35(3)	42(3)	4(3)	3(2)	-3(2)
C(18)	21(3)	26(3)	41(3)	2(2)	-2(2)	-3(2)
C(19)	25(3)	24(3)	36(3)	3(2)	0(2)	0(2)
C(20)	28(3)	19(2)	37(3)	0(2)	-3(2)	-2(2)
C(21)	23(3)	24(3)	37(3)	1(2)	-1(2)	-1(2)
C(22)	22(3)	22(3)	47(3)	0(2)	-4(2)	1(2)
C(23)	31(3)	31(3)	49(3)	1(3)	0(3)	8(2)
C(24)	26(3)	30(3)	48(3)	2(3)	-2(3)	1(2)
C(25)	23(3)	27(3)	43(3)	2(2)	-4(2)	-3(2)
C(26)	26(3)	22(2)	32(3)	6(2)	0(2)	0(2)

Table S5. Hydrogen coordinates ($\times 10^4$) and isotropic displacement parameters ($Å^2 \times 10^3$) for **1H**.

	x	y	z	U(eq)
H(1)	6360(20)	2660(50)	7130(100)	70(20)
H(2)	4976	4320	5414	41
H(3)	5244	5718	3559	38
H(5)	7469	5047	3944	32
H(8)	8354	4140	4891	37
H(9)	9294	2992	5965	41
H(10)	8940	1514	7676	44
H(11)	7680	1298	8322	40
H(12A)	6934	6209	1586	38
H(12B)	6109	6720	1852	38
H(15)	8057	6230	2055	36
H(16)	9339	6429	2391	41
H(17)	9836	7879	3983	41
H(18)	9027	9133	5182	35
H(20)	7762	9800	5750	34
H(22)	6499	10530	6311	37
H(23)	5201	10430	6027	44
H(24)	4666	9023	4398	42
H(25)	5399	7703	3191	37

Table S6. Torsion angles [°] for **1H**.

O(1)-C(1)-C(2)-C(3)	-179.8(5)
C(6)-C(1)-C(2)-C(3)	0.2(8)
C(1)-C(2)-C(3)-C(4)	-1.4(8)
C(2)-C(3)-C(4)-C(5)	1.9(7)
C(2)-C(3)-C(4)-C(12)	-178.7(5)
C(3)-C(4)-C(5)-C(6)	-1.3(7)
C(12)-C(4)-C(5)-C(6)	179.4(4)
C(4)-C(5)-C(6)-C(1)	0.1(7)
C(4)-C(5)-C(6)-C(7)	178.8(5)
O(1)-C(1)-C(6)-C(5)	-179.5(5)
C(2)-C(1)-C(6)-C(5)	0.5(7)
O(1)-C(1)-C(6)-C(7)	1.8(7)
C(2)-C(1)-C(6)-C(7)	-178.2(5)
C(11)-N(1)-C(7)-C(8)	0.2(7)
C(11)-N(1)-C(7)-C(6)	179.9(5)
C(5)-C(6)-C(7)-N(1)	-177.6(4)
C(1)-C(6)-C(7)-N(1)	1.0(7)
C(5)-C(6)-C(7)-C(8)	2.0(7)
C(1)-C(6)-C(7)-C(8)	-179.4(5)
N(1)-C(7)-C(8)-C(9)	0.4(8)
C(6)-C(7)-C(8)-C(9)	-179.2(5)
C(7)-C(8)-C(9)-C(10)	0.2(8)
C(8)-C(9)-C(10)-C(11)	-1.3(8)
C(7)-N(1)-C(11)-C(10)	-1.5(8)
C(9)-C(10)-C(11)-N(1)	2.0(9)
C(3)-C(4)-C(12)-C(13)	106.9(5)
C(5)-C(4)-C(12)-C(13)	-73.7(6)
C(4)-C(12)-C(13)-C(14)	92.5(6)
C(4)-C(12)-C(13)-C(26)	-85.3(6)
C(26)-C(13)-C(14)-C(15)	-177.3(5)
C(12)-C(13)-C(14)-C(15)	4.9(8)
C(26)-C(13)-C(14)-C(19)	2.8(7)
C(12)-C(13)-C(14)-C(19)	-175.0(4)
C(13)-C(14)-C(15)-C(16)	-178.9(5)

C(19)-C(14)-C(15)-C(16)	1.0(8)
C(14)-C(15)-C(16)-C(17)	0.1(8)
C(15)-C(16)-C(17)-C(18)	-0.7(8)
C(16)-C(17)-C(18)-C(19)	0.2(8)
C(17)-C(18)-C(19)-C(20)	179.6(5)
C(17)-C(18)-C(19)-C(14)	1.0(8)
C(13)-C(14)-C(19)-C(20)	-0.3(7)
C(15)-C(14)-C(19)-C(20)	179.8(5)
C(13)-C(14)-C(19)-C(18)	178.4(5)
C(15)-C(14)-C(19)-C(18)	-1.5(7)
C(18)-C(19)-C(20)-C(21)	179.5(5)
C(14)-C(19)-C(20)-C(21)	-1.8(8)
C(19)-C(20)-C(21)-C(22)	-179.1(5)
C(19)-C(20)-C(21)-C(26)	1.4(8)
C(20)-C(21)-C(22)-C(23)	179.7(5)
C(26)-C(21)-C(22)-C(23)	-0.8(8)
C(21)-C(22)-C(23)-C(24)	-0.9(8)
C(22)-C(23)-C(24)-C(25)	1.7(8)
C(23)-C(24)-C(25)-C(26)	-0.7(8)
C(14)-C(13)-C(26)-C(25)	176.6(5)
C(12)-C(13)-C(26)-C(25)	-5.5(7)
C(14)-C(13)-C(26)-C(21)	-3.3(7)
C(12)-C(13)-C(26)-C(21)	174.6(5)
C(24)-C(25)-C(26)-C(13)	179.0(5)
C(24)-C(25)-C(26)-C(21)	-1.1(7)
C(20)-C(21)-C(26)-C(13)	1.2(7)
C(22)-C(21)-C(26)-C(13)	-178.3(5)
C(20)-C(21)-C(26)-C(25)	-178.7(5)
C(22)-C(21)-C(26)-C(25)	1.8(7)

Table S7. Hydrogen bond metrical parameters for **1H**.

D-H...A	d(D-H)	d(H...A)	d(D...A)	<(DHA)
O(1)-H(1)...N(1)	1.02(3) Å	1.62(4) Å	2.566(5) Å	153(7)°

3. DFT calculations.

All calculations were performed with Gaussian09.[1] All calculations were performed at the B3LYP/6-31++G(d,p) level of theory with acetonitrile solvent modeled by a polarizable continuum model (C-PCM). The geometry optimization was performed including the ultrafine keyword and was confirmed to be a local minimum by vibrational analysis (NImag = 0). The sum of electronic and zero-point energies for the optimized local minimum of **1H** is -1131.922852 hartrees.

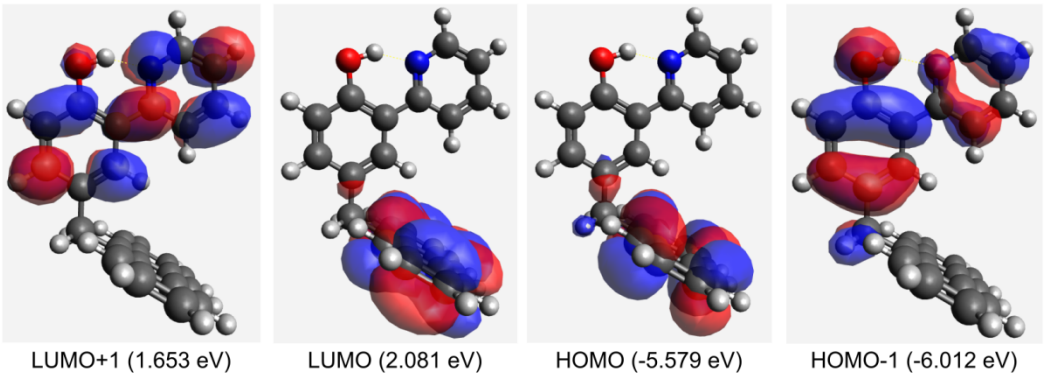

Figure S16. Representation of frontier molecular orbitals for **1H** local minima and their energies.

Table S8. Cartesian coordinates for optimized local minimum of **1H**.

1H in MeCN			
O	-4.58558	-1.49408	-0.97432
H	-4.84898	-0.78583	-0.3046
N	-4.43473	0.428138	0.695525
C	1.052963	-1.21447	-1.8419
H	1.416185	-2.24024	-1.95929
H	1.202492	-0.76034	-2.82655
C	1.912721	-0.49465	-0.81846
C	2.260954	0.867945	-0.99925
C	1.7867	1.657968	-2.10163
H	1.118015	1.215502	-2.83054
C	2.145617	2.974969	-2.25121
H	1.765614	3.543788	-3.09479
C	3.009434	3.607933	-1.30955
H	3.285642	4.649166	-1.44625
C	3.480809	2.89908	-0.23517
H	4.134884	3.369481	0.494344
C	3.123932	1.525254	-0.03877
C	3.59449	0.812185	1.068741
C	3.239028	-0.52507	1.278671
C	3.713721	-1.24363	2.423416
H	4.363223	-0.72502	3.123778
C	3.358199	-2.55055	2.637364

H	3.723022	-3.08428	3.509829
C	2.500704	-3.21224	1.710269
H	2.215326	-4.24485	1.888959
C	2.030294	-2.55829	0.597639
H	1.370937	-3.08788	-0.07975
C	2.379178	-1.1925	0.325106
C	-1.07484	-0.4015	-0.66394
H	-0.46049	0.319227	-0.13764
C	-0.44642	-1.26802	-1.55361
C	-1.24606	-2.20755	-2.23123
H	-0.78586	-2.90347	-2.92866
C	-2.61719	-2.26212	-2.02281
H	-3.23325	-2.98798	-2.54474
C	-3.24392	-1.38103	-1.12622
C	-2.46597	-0.42439	-0.41882
C	-3.08954	0.514528	0.544766
C	-2.36162	1.464452	1.289825
H	-1.28748	1.54852	1.188248
C	-3.03137	2.306429	2.170661
C	-4.41927	2.201901	2.309862
H	-4.97386	2.841542	2.987243
C	-5.0753	1.241576	1.546871
H	-6.15209	1.110746	1.61198
H	-2.47405	3.039365	2.745891
H	4.244933	1.308991	1.784652

4. Fluorescence measurements.

Samples were prepared in a nitrogen atmosphere glovebox. Liquid samples for ambient-temperature studies were prepared in Teflon-sealed quartz cuvettes (1 cm x 1 cm). Samples of triads **1H** and **1Me** (9.0 μM) were prepared in acetonitrile with 2% methanol by volume. Samples of **1D** were prepared from solutions of **1H** (9.0 μM) in acetonitrile with 2% methanol-d_4 by volume. Liquid samples for temperature dependence studies were loaded into quartz capillaries (1 mm inner diameter, 2 mm outer diameter, 2 cm long) sealed with rubber septa. These samples contained triad **1H** or **1Me** (85 μM) in 2-MeTHF or MeCy with 3% methanol or methanol-d_4 by volume. Thin films were prepared by adding triad **1H** (1.2 mg, 3.3 μmol) to a mixture of PMMA in toluene (65 mg/mL, 200 μL) and stirring at 70 °C for 20 min. This solution was spin-coated onto a sapphire plate.

All samples for temperature-dependence studies were mounted using custom-fabricated copper blocks. Temperature was controlled by a He-flow cryostat or by a nitrogen-filled chamber with a heating apparatus.

Time-resolved fluorescence measurements were performed using the frequency-doubled output of a mode-locked Ti:sapphire oscillator with a pulse duration of 150 fs. (Coherent Mira HP), resulting in excitation wavelengths of 361-364 nm. The Ti:sapphire repetition rate was slowed from 76 MHz to 4.75 MHz using a pulse picker (Coherent). Time-resolved fluorescence data were collected using a streak camera (Hamamatsu C10627) in combination with a grating spectrometer (Acton, 0.3 m, 50 g/mm, 500 nm blaze).

The streak camera data, collected over both 1 ns and 50 ns windows for all samples, were integrated over all fluorescence wavelengths to produce fluorescence decay traces as a function of time. The instrument response function width was measured using the residual scattered signal from the excitation pulse. Lifetimes were extracted from the time traces using Gaussian deconvolution fits to single or double exponentials in Igor Pro.

Table S9. Data from fluorescence quenching spectroscopy: Temperature dependence of the fast component of the fluorescence decay lifetimes. The time constant for the slow component of the biexponential decay was consistently found to be 8 ns across multiple conditions, and was thus fixed at 8 ns for the calculation of the tau values below.

1H in 2-MeTHF	
T (K)	tau (ps)
5.5	86.8
5.5	86.9
5.5	88.6
5.5	94.1
7	80.4
10	88.3
10	90.1
13	85.7
20	83.3
20	88.9
24	84.4
40	84.7
40	88.3
60	86.0
60	87.4
80	83.6
85	74.8
145	91.3
175	80.8
175	84.1
185	80.3
200	88.7
200	81.5
200	76.1
210	78.3
220	75.3
230	91.7
240	78.0
250	72.4
250	71.7
260	68.0
270	66.8
280	61.5
290	65.3
300	59.9
300	56.4
300	56.3
300	58.9
310	54.0
320	54.7
330	51.3
340	50.3
350	50.1

1D in 2-MeTHF	
T (K)	tau (ps)
5.5	276.8
7	215.7
10	204.3
13	220.0
20	260.6
24	212.7
40	198.4
60	211.6
85	200.8
125	358.7
145	515.3
175	317.9
175	382.0
185	361.9
200	275.2
200	306.6
210	280.1
220	279.6
230	255.6
240	241.0
250	215.1
250	228.0
260	230.9
270	217.3
280	195.7
290	189.4
300	167.3
300	176.2
300	152.4
310	133.6
320	124.3
330	116.0
340	102.4
350	89.6

1H in PMMA	
T (K)	tau (ps)
5.5	151.5
10	160.9
20	156.6
40	152.5
60	150.2
85	146.8
95	140.2
105	138.8

115	145.8
125	132.5
145	124.4
175	120.8
200	112.9
250	112.7
300	92.4

1H in MeCy	
T (K)	tau (ps)
5.5	88.0
10	82.8
20	84.0
40	79.9
60	76.6
85	84.0
105	63.8
125	81.9
145	101.5
175	113.6
200	134.8
250	111.4
300	86.4

1Me in 2-MeTHF	
T (K)	tau (ns)
5.5	9.8
10	9.6
20	9.3
40	9.1
60	8.9
80	9.1
125	9.0
145	8.9
175	9.2
200	9.4
250	8.2
300	6.2

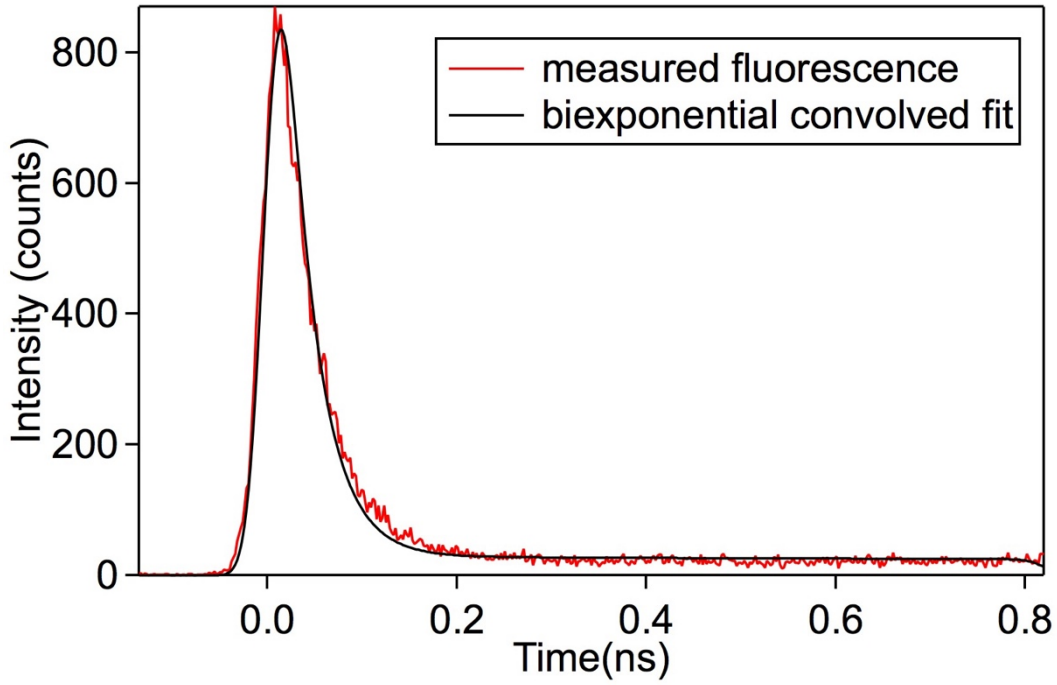

Figure S17. Example of fluorescence decay and biexponential fit: compound **1H** in MeCN at room temperature.

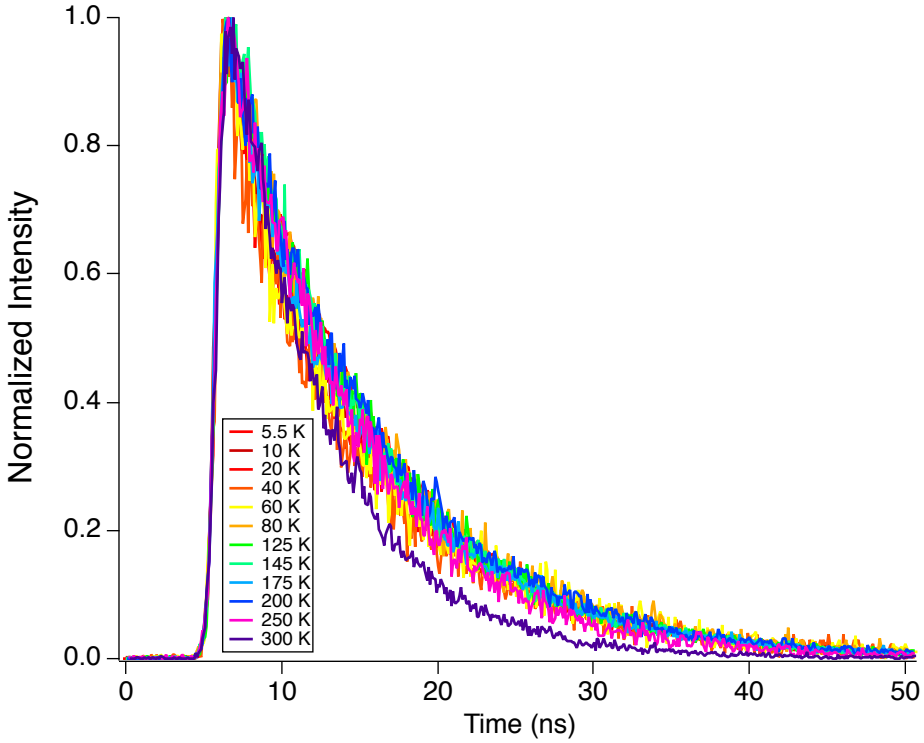

Figure S18. Temperature dependence study of fluorescence decay rates for compound **1Me** in 2-MeTHF.

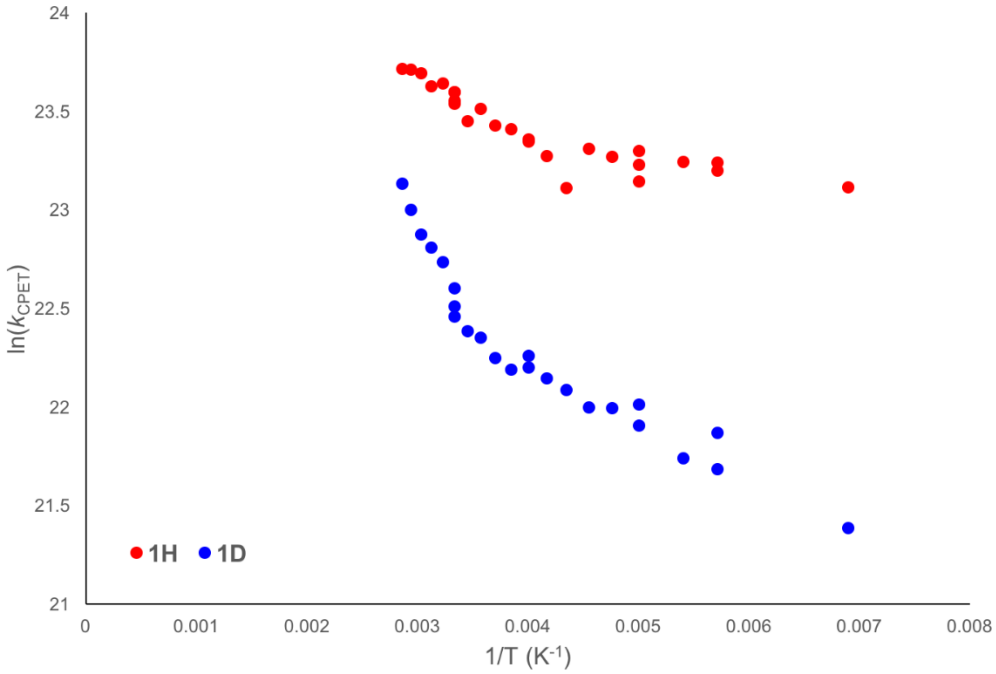

Figure S19. Arrhenius plot for MS-CPET of compounds **1H** and **1D** in 2-MeTHF, expanded from Figure 4B to show detail of the high temperature regime (145 – 350 K).

5. Transient absorption spectroscopy.

The transient absorption experiments reported were repeated several times using different instruments and different sources of white light generation. The procedures and results for the experiments are described below. Overall, the replicability is very good. There is a small shoulder at ~630 nm visible in one dataset that is likely obscured by the breadth of the main peak at 590 nm in the other. Similar broadening could account for the small differences in the long-lived component spectrum as well. In general, the data are more challenging to obtain closer to the fundamental of the 800nm Ti: sapphire output that is pumping the white-light generation.

Procedure A (Seattle, WA, USA):
Samples were prepared in a nitrogen atmosphere glovebox and loaded into quartz cuvettes (2 mm pathlength x 1 cm) with stir bars and septum-sealed screw caps. The solutions contained triad **1H** or **1Me** (96 μM) in MeCN and were measured at ambient temperatures.

The 800 nm output (pulse duration ~50 fs, repetition rate 1 kHz) from a Ti:sapphire laser system (Coherent, Libra) was used to generate both pump and probe beams for transient absorption measurements. This output was split using a 75/25 beam splitter. The higher-intensity beam was directed into the optical parametric amplifier (OPA) and frequency doubled to provide the 365 nm pump pulse. The lower intensity beam was used for probe white light generation. A white light continuum (WLC) was generated by focusing the Ti:sapphire output beam onto a sapphire crystal. A linear ND filter was used to split the WLC into a probe beam and a reference beam. The change in transmittance of the sample was measured with a CMOS detector. A short pass filter was used to attenuate the residual 800 nm fundamental beam. An electronic chopper (500 Hz) was used to collect pump on-pump off measurements. Surface Xplorer software (Ultrafast Systems) was used to collect the absorption spectra, and OriginLab OriginPro 9.1.0 was used for initial processing, analysis, and plotting of the data. Global analysis with a three-component sequential model was carried out using the Globe Population Dynamics Modelling Toolbox by J.J. van Thor and co-workers in MatLab.

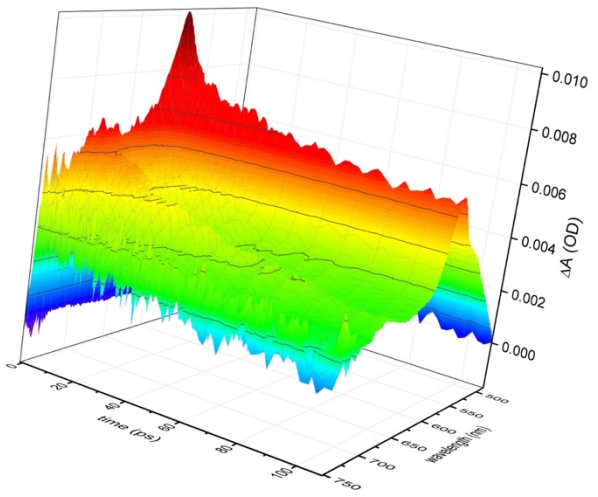

Figure S20. Transient absorption spectra (procedure A) of compound **1Me** in MeCN up to 100 ps after photoexcitation.

Procedure B (Uppsala, Sweden):
Samples of **1H** were prepared in quartz cuvettes (1 mm pathlength × 1 cm) and septum-sealed screw caps. The concentration was adjusted in order to give an absorbance of 0.6 at 365 nm. The solutions were measured at ambient temperature.

The femtosecond transient absorption apparatus is described in Petersson *et al.* [2] Briefly, the output from a Coherent Legend Ti:sapphire amplifier (1 kHz, 800 nm, fwhm 100 fs) was split into a pump and a probe. The pump beam was directed into an optical parametric amplifier (TOPAS-White, Light Conversion), and then frequency doubled in a second harmonic generator (TOPAS SHS, Light Conversion) to obtain the 365 nm excitation wavelength, which was then separated from the remaining visible light with dichroic mirrors. The output was passed through a mechanical chopper, blocking every second pulse, and was later focused in the sample cell. Before the sample cell, part of the pump light was directed to a diode in order to reject pulses with intensities that fall outside of an optimal range. The white-light supercontinuum probe was obtained by focusing part of the 800 nm light on a moving 3 mm thick CaF_2 plate (for 380-710 nm probe light) or a fixed 3 mm thick sapphire window (for 420-750 nm probe light). The probe spectrum was recorded on a silicon diode array. Instrumental response time depends on pump and probe wavelengths but was typically ~150 fs. The transient absorption spectra at different times were recorded for the sample by scanning the delay of the probe beam relative to the pump from -15 ps to 2 ns with the help of an optical delay line. The samples were kept in constant motion during the measurement. This procedure was repeated 5 times for each sample. Global analysis of the time-resolved data was performed using a sequential three-component exponential decay scheme in a least-squares fitting performed with the R package TIMP and its GUI Glotaran.[3,4]

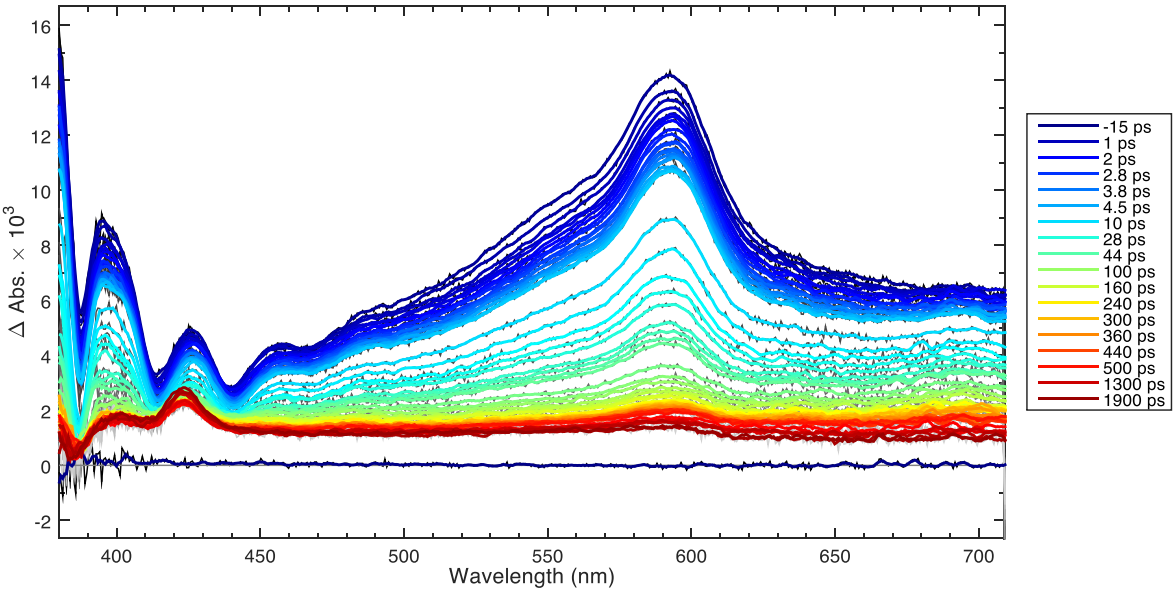

Figure S21. Transient absorption spectra (procedure B) of compound **1H** in MeCN up to 2.0 ns after photoexcitation. Observation wavelength range generated by CaF_2: 380 – 710 nm. After photoexcitation and up to a few hundreds of picoseconds, both transient absorption and stimulated emission contribute to the transient spectra between 390 and 480 nm. Only absorption is present throughout the range between 400 and 710 nm at times longer than a few hundreds of picoseconds.

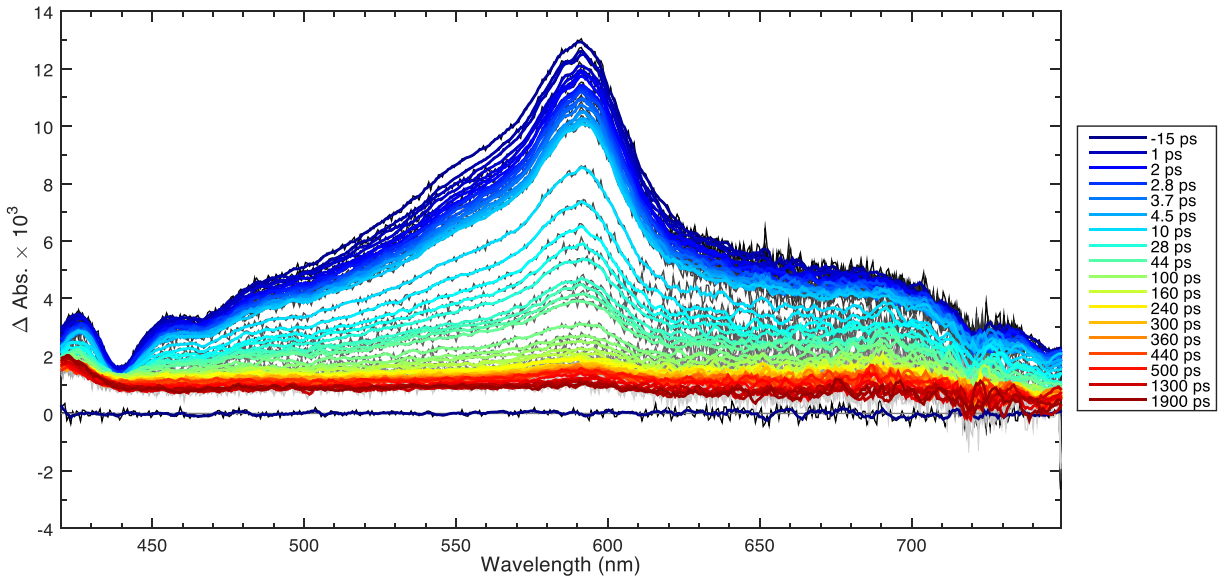

Figure S22. Second transient absorption data set using procedure B, of compound **1H** in MeCN up to 2.0 ns after photoexcitation. Observation wavelength range generated by sapphire: 420 – 750 nm. The transient spectra show similar behavior as those in Figure S21.

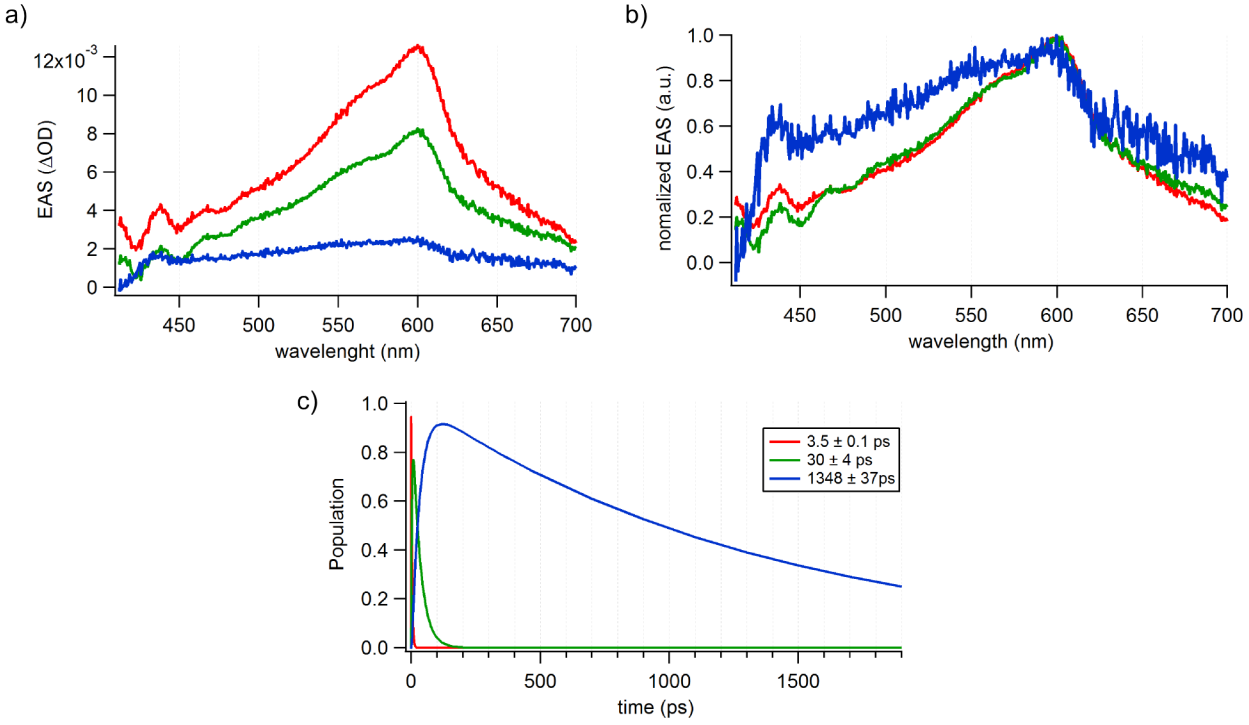

Figure S23. a) Evolution-associated spectra (EAS) from a global analysis of the transient absorption of **1H** in MeCN upon photoexcitation (procedure B). Delay time range -15 ps to 2 ns. b) Normalized EAS. c) Time evolution of the populations for the three species in the global analysis. *Red*: instantaneously formed species, 3.5 ± 0.1 ps decay. *Green*: first intermediate species, 3.5 ± 0.1 ps rise, 30 ± 4 ps decay. *Blue*: second intermediate species, 30 ± 4 ps rise, 1348 ± 37 ps decay. The second intermediate species does not decay completely to the ground state within the 2 ns time window of the experiment.

6. References.

(1) Gaussian 09, R. C., M. J. Frisch, G. W. Trucks, H. B. Schlegel, G. E. Scuseria, M. A. Robb, J. R. Cheeseman, G. Scalmani, V. Barone, B. Mennucci, G. A. Petersson, H. Nakatsuji, M. Caricato, X. Li, H. P. Hratchian, A. F. Izmaylov, J. Bloino, G. Zheng, J. L. Sonnenberg, M. Hada, M. Ehara, K. Toyota, R. Fukuda, J. Hasegawa, M. Ishida, T. Nakajima, Y. Honda, O. Kitao, H. Nakai, T. Vreven, J. A. Montgomery, Jr., J. E. Peralta, F. Ogliaro, M. Bearpark, J. J. Heyd, E. Brothers, K. N. Kudin, V. N. Staroverov, T. Keith, R. Kobayashi, J. Normand, K. Raghavachari, A. Rendell, J. C. Burant, S. S. Iyengar, J. Tomasi, M. Cossi, N. Rega, J. M. Millam, M. Klene, J. E. Knox, J. B. Cross, V. Bakken, C. Adamo, J. Jaramillo, R. Gomperts, R. E. Stratmann, O. Yazyev, A. J. Austin, R. Cammi, C. Pomelli, J. W. Ochterski, R. L. Martin, K. Morokuma, V. G. Zakrzewski, G. A. Voth, P. Salvador, J. J. Dannenberg, S. Dapprich, A. D. Daniels, O. Farkas, J. B. Foresman, J. V. Ortiz, J. Cioslowski, and D. J. Fox, Gaussian, Inc., Wallingford CT, 2010.

(2) Petersson, J.; Eklund, M.; Davidsson, J.; Hammarström, L. *The Journal of Physical Chemistry B* **2010**, *114*, 14329-14338.

(3) Mullen, K. M.; van Stokkum, I. H. M. *Journal of Statistical Software* **2007**, *18*, 46.

(4) Snellenburg, J. J.; Laptenok, S.; Seger, R.; Mullen, K. M.; van Stokkum, I. H. M. *Journal of Statistical Software* **2012**, *49*, 22.